processes

MDPI

*Article*

# How to (Not) Make a Perovskite Solar Panel: A Step-by-Step Process

**Luigi Angelo Castriotta [1,*] and Enrico Leonardi [2]**

[1] CHOSE (Centre for Hybrid and Organic Solar Energy), Department of Electronic Engineering, University of Rome "Tor Vergata", 00133 Rome, Italy
[2] Greatcell Italy, Greatcell Solar Italia, Viale Castro Pretorio 122, 00185 Rome, Italy
* Correspondence: luigi.angelo.castriotta@uniroma2.it

**Abstract:** To date, scientific research on perovskite solar cells (PSCs) and modules (PSMs) has been carried out for more than 10 years. What is still missing in the market potential of this technology is a complete description of the materials needed to connect and fabricate PSMs in order to build a perovskite solar panel. Starting from the state-of-the-art perovskite solar modules, the material and design optimization using different substrates and architecture types, and ending in the lamination of the panel, this work focusses on the study of the feasibility of the fabrication of a perovskite solar panel. A complete description of all steps required will be provided in detail.

**Keywords:** perovskite solar panel; photovoltaic upscaling; perovskite practical issues



**Citation:** Castriotta, L.A.; Leonardi, E. How to (Not) Make a Perovskite Solar Panel: A Step-by-Step Process. *Processes* **2022**, *10*, 1980. https://doi.org/10.3390/ pr10101980

Academic Editors: Sheng Hsiung Chang and Kian Jon Chua

Received: 1 September 2022
Accepted: 20 September 2022
Published: 1 October 2022



## 1. Introduction

Third-generation perovskite solar cells have boosted performance up to 25.7%, which is almost identical to the efficiency level for conventional silicon-based solar cells [1,2]. However, these results stem from laboratory tests on millimeter-sized samples in simulated conditions; they do not account for outdoor environmental factors, which are significant given that this is where perovskite-based devices are utilized. This implies that the potential degradation and deterioration over time due to these factors is not accounted for. Only a few works start to discuss the potential application of perovskite technology in outdoor conditions [3–5], and only the work by Pescetelli et al. included a detailed description of all materials required, from perovskite modules to the lamination process [6]. To make correct decisions, it is important to know how each different module design will function at the large scale in the real world. This is why we believe that a detailed description of how to fabricate a perovskite solar panel is important in the research community, as well as establishing the steps to be taken to limit any further issues, in such a way as to "not" make irreparable mistakes. Hence, we focus our work on the material choice, based on the results obtained in previous works [7–9], and then describe what is needed for the panel fabrication process. Our aim is to guide the reader through the processes needed to build a perovskite solar panel, a fabrication procedure totally different from that of perovskite solar cells [10], in which other techniques and optimizations are used, focusing more on the scientific aspect of the technology, rather than the engineering issues, and how to address limits.

## 2. Materials and Methods

Dimethylformamide (DMF, anhydrous; Sigma-Aldrich, St. Louis, MO, USA), dimethyl sulfide (DMSO, anhydrous; Sigma-Aldrich), chlorobenzene (CB, anhydrous; Sigma-Aldrich), isopropanol (IPA, anhydrous; Sigma-Aldrich), C60 fullerene (C60, 99.5%; Solenne, Groningen, The Netherland), bathocuproine (BCP, 96%; Sigma-Aldrich), formamidinium iodide (FAI, 99.99%; Greatcell solar, Bomen, Australia), cesium iodide (CsI, 99.99%; Sigma-Aldrich),

lead bromide (PbBr2; TCI), and lead iodide (PbI2; TCI) were purchased and used without further purification.

**Perovskite Preparation.** $PbI_2$ (1 M), CsI (0.1 M), and FAI (with a weight ratio of FAI:$PbI_2$-CsI 1:20) were dissolved in DMF (0.876 mL) and DMSO (86 µL); FAI and FABr (0.4 M $mL^{-1}$), with FABr molar fractions of 20 mol %, was dissolved in IPA. The final perovskite precursor ratio was Cs0.1FA0.9Pb(I0.94Br0.06)3.

**Modules Fabrication.** Perovskite solar modules with an active area of 201 $cm^2$ were realized on fluorine-doped tin oxide (FTO) conductive glass (Pilkington, 8 $\Omega_{\square}^{-1}$) patterned through a raster scanning laser. The P1 process, designing 16 series of connected cells, was performed for the module layout using the same parameters (λ = 355 nm, Nd:YVO4 pulsed at 80 kHz, fluence = 648 mJ $cm^{-2}$). The patterned substrates were cleaned in an ultrasonic bath by sequential washing in detergent with deionized water, acetone, and isopropanol (10 min for each step). The patterned substrates were initially set at 20 × 30 $cm^{-2}$ for to facilitate the optimization of the PTAA and perovskite layer by a semi-automatized blade and slot die coater with three different drying step methods (fan, hot air, and IRA), called "Charon" designed by Cicci Research srl, and subsequentially cut into 20 × 20 $cm^{-2}$ sections. The deposition process was carried out in ambient air. Subsequently, 10-min UV–ozone treatment was performed prior to layer processing. A PTAA solution in anisole (5 mg/mL, 300 µL) was injected into one side of the substrate with a syringe forming a uniform meniscus between the substrate and the blade: the deposition was performed in air with relative humidity of 20 to 30%, using a 100-µm blade height and 5 mm/s speed, followed by annealing at 100 °C for 10 min. Subsequently, the samples were exposed to UV–ozone treatment for 10 min, and then transferred back for perovskite layer deposition. Perovskite deposition was performed under controlled humidity at 20 to 30% using "Charon", and the plate of the machine was kept constant at 30 °C. In the first step, the blade height was fixed at 100 µm, and the precursor solution ($PbI_2$, CsI, and FAI in DMF/DMSO 9:1) was continuously stirred at room temperature just before the deposition stage. Precursor solution (300 µL) was injected into one side of the substrate with a syringe forming a uniform meniscus between the substrate and the blade, after which the plate moved at a fixed speed of 10 mm/s. Once the substrate crossed the blade system, an air drying system set at 65 °C was used, with a fixed pressure of 125 L $min^{-1}$. Immediately after the drying step, the substrate was placed back in its starting position. During the second step, a precursor solution, made of FAI and FABr in IPA, was kept in a syringe dispensing the slot die; the initial flow rate was adjusted to form a uniform meniscus between the substrate and the slot die head placed at 70 µm from the substrate, and once the meniscus was formed, the flow rate was kept at 500 µL $min^{-1}$ and the plate moved at a fixed speed of 20 mm/s. Once the substrate crossed the slot die system, an air drying system, set at room temperature with a fixed pressure of 100 L $min^{-1}$, and a couple of infrared lights were used for 5 s; after that, the substrate was placed on a hot plate at 130 °C for 40 min. Infrared lights were composed of two emitters of 400 mm length with two kW total electrical power. The lamps were composed of infrared quartz with a fast medium wave emitter with peaks in the range of 1.6–2.0 µm and a working emitter temperature at 1462 °C. Blade, slot die, and drying apparatuses were placed at a specific distance from each other, and were activated and controlled by software during the deposition.

On top of the perovskite layer, 30 nm of C60 as ETL and 8 nm of BCP as a buffer layer were thermally evaporated at a vacuum pressure of $10^{-6}$ mbar. Finally, as the back-contact, 100 nm of Au electrode was deposited on top of the layers by thermal evaporation at $10^{-5}$ mbar. To form interconnections in the module, P2 and P3 were performed (λ = 355 nm, Nd:YVO4 pulsed at 80 kHz, $fluence^{P2}$ = 195 mJ $cm^{-2}$, $fluence^{P3}$ = 206 mJ $cm^{-2}$) following a similar procedure reported elsewhere [11]. Scanning electron microscopy (SEM) experiments were performed using a TESCAN Analytics VEGA instrument. Modules were measured with an ABET Sun 2000 class A sun simulator, calibrated with an Eko MS-602 pyranometer.

The choice of material plays an important role when dealing with perovskite solar panels: we need to take into consideration all the fabrication processes we might use for each step, and reduce, as much as possible, the lengthy processes that might not be beneficial for the outcoming result. The size of the panel and number of the modules are the first choices to make: for big area substrates larger than ~0.5 $m^2$, glass can be hard to handle, and an additional transport equipment is needed for the final installation. We decided to make a panel starting with a glass size of 65 × 85 $cm^2$, resulting in a total area of 0.55 $m^2$. The number of modules to use strongly depends on the limit size of the process applied for the layer deposition step of the modules. In our case, we decided to produce a module of 20 × 20 $cm^2$, and, to connect those modules in a 0.5 $m^2$ panel, we needed to fabricate 12 modules. The two main bottlenecks when choosing the module size to incorporate in a panel are the spin coating process and the sintering step for the ETL layer in a NIP architecture: spin coating is a process in which a large quantity of solution is wasted, and we strongly avoid this technique to use less material solution for the deposition. The sintering process, occurring at sizes larger than 100 $cm^2$, creates cracks over 300 °C. For this reason, we chose to work with PIN structures: the layer deposition steps do not require high temperature processes, and allow one to obtain modules that are more stable over time, as already tested in our previous work [8,12]. A perovskite solar panel is stable over time if all the modules incorporated are stable as well: although this may seem obvious, it might happen that, even though the modules are working correctly and appear to be stable, there is a missing connection among modules that causes failures in the photovoltaic panel, rendering it useless. The attention at this stage is focused on the engineering part of the process, whereas for the module fabrication stage, the focus turns to the chemistry and material science aspects.

## 3. Results

### *3.1. Substrate and Transparent Electrode*

The first step when preparing the fabrication of a perovskite solar panel is to choose the substrate: this choice depends mainly on the application and installation that we envision for the final product. Flexible panels have a wide range of applications, ranging from smart furniture to IoT to transportation; however, there are some main drawbacks to consider, such as the low temperature needed for the fabrication due to the use of plastic substrates [13]. In rigid substrates, on the other hand, fabrication can be accomplished at higher temperatures also required for the lamination process of the final panel. For this reason, we decided to address our fabrication process using rigid substrates. In the perovskite research community, two substrates with coated transparent electrodes are mainly available and used in the market; these are fluorine-doped tin oxide (FTO) and indium-doped tin oxide (ITO), both commercially available on glass.

Another important parameter to consider when fabricating large devices is the thickness of the substrate itself; two main thicknesses have been considered in this work, 1.1 mm and 2.2 mm. Strong mechanical parameters of the glass allow us to handle the 20 × 20 $cm^2$ module even at temperatures above 100 °C for 2.2 mm thickness, whereas we discovered that additional care is required for thinner substrates, becoming more fragile and easier to break, not only at module size but also when assembled in areas of A4 size and beyond [14]. Glass/FTO is generally commercially available at 2.2 mm thickness, whereas Glass/ITO is typically available at 1.1 mm thickness. This thickness might be crucial for the panel fabrication. The roughness of the transparent electrode should be as reduced as possible, especially when conduct work using PIN architecture: common hole transport layers used for this architecture are generally thinner than those used for the electron transport layer in NIP structures, both of which are generally deposited on top of the transparent electrode [15]. A trade-off between the robustness of the glass/transparent electrode and the roughness swayed our choice in favor of the glass/FTO substrate.

### 3.2. Perovskite

The perovskite layer represents the most delicate layer choice at this stage, since it is the absorbent material and the layer responsible for proper current generation in the photovoltaic device. The intrinsic stability of the material guarantees better overall stability of the device, and it is noted that the methylammonium (MA) cation is the most volatile material that might cause degradation of the perovskite crystal [16,17]. Double-cation perovskite, such as CsFA perovskite, demonstrates promising stability under light soaking for both small and module-like areas [18,19]. To maintain the optimization step we obtained in our previous work [7], we decided to deposit CsFA-based perovskite into the air using "Charon", a semi-automatic blade and slot die coater with three different drying step methods (fan, hot air, and infrared annealing), designed by Cicci Research srl. Perovskite films are shown in Figure 1: thickness across the module was checked using a profilometer. The results show that the modules had a uniform perovskite layer (see Figure 1), with thickness values ranging from 400 to 600 nm from the beginning to the end of the deposition stage: this gradient, and not homogenous deposition, might be due to the air environment used, as a slight change in relative humidity might cause variations in perovskite crystal formation. Nevertheless, we decided to proceed with the fabrication of the panel in order to understand all of the possible steps to consider.

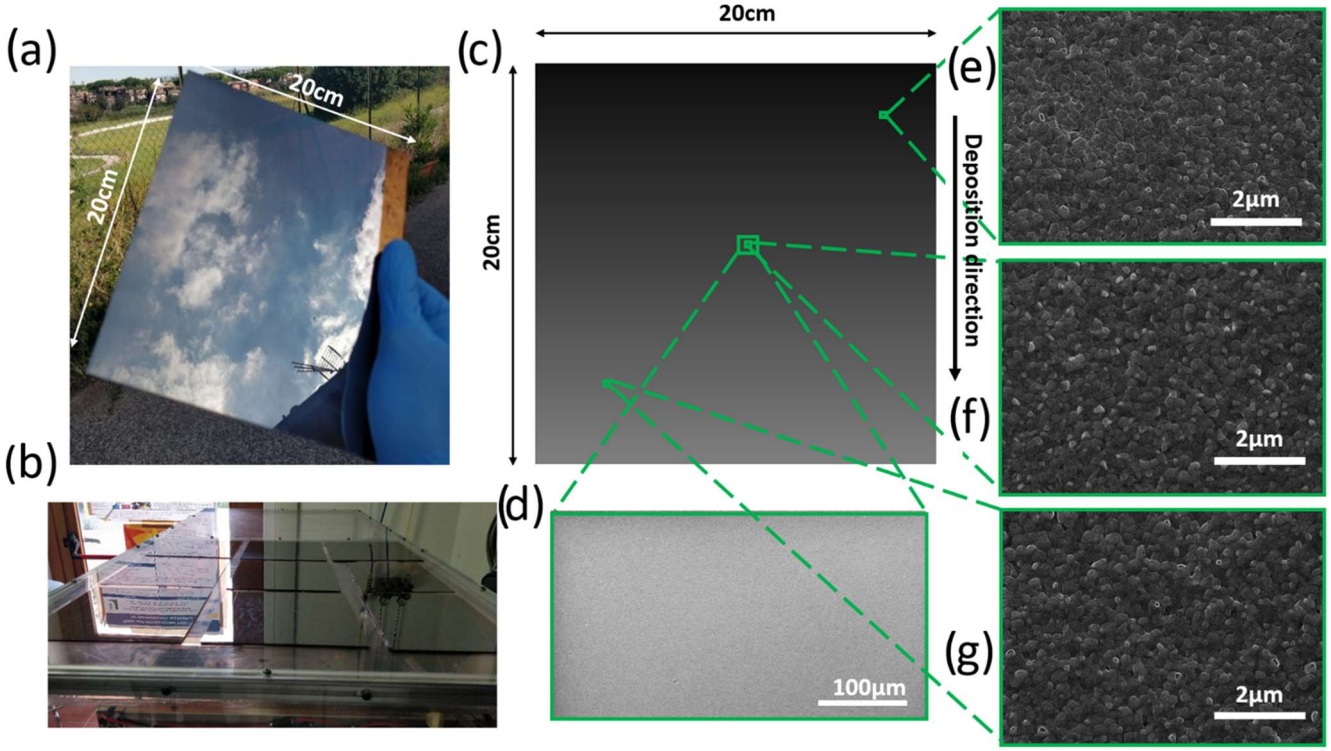


**Figure 1.** (**a**,**b**) Images of CsFA perovskite depositions in an air environment (with relative humidity of 20–30%) using a semi-automatic blade and slot die coater. (**c**) Scheme of the perovskite substrate size to show where SEM images where taken. (**d**–**g**) SEM images with 100 µm (**d**) and 2 µm (**e**–**g**) scale bars.

### 3.3. Selective Transporting Layers

The choice of selective transport layers mainly depends on the architecture of the perovskite device: for the NIP mesoscopic structure, the major bottleneck is the need for high temperatures for the sintering process of the $TiO_2$ electron transport layer (ETL). When using a large substrate, such as a 20 × 20 $cm^2$ module, the possibility of breaking the glass at temperatures over 300 °C is exponentially elevated; this is one of the reasons we discarded this method. In the PIN structure, the annealing procedure requirements are less elevated, and for some specific layers, it does not even occur [20]. A separate paragraph for ETL and HTL further discusses this aspect.

3.3.1. Hole Transport Layer

It is necessary to start depositing the HTL on top of the transparent electrode when choosing the PIN structure for panel fabrication. Glass/FTO substrate should be treated with adequate cleaning and, for some layers, UV–ozone treatment to cure and increase wettability of the substrate [21]. There are many types of layers that we might use, but depending on the work carried out previously, we decided to use PTAA for several reasons: it requires low-temperature annealing (100 °C), and its solution is processable with non-hazardous solvents, such as anisole; the deposition of this polymer has been optimized in our previous work using PET substrates [8,22,23]. An ellipsometry study was conducted, as shown in Figure 2. The results show that PTAA layer deposition is uniform along the deposition area with dimensions of 250 × 200 $mm^2$, with an average thickness of 7.6 ± 0.4 nm. As we observe in Table 1, roughness of FTO varied from 12 to 17 nm: in order to achieve a uniform deposition layer on top of the roughness, we conducted the PTAA deposition process, increasing the blade height from 100 to 150 µm. PTAA deposited in this way showed uniform deposition along the area. The starting glass/FTO substrate used had dimensions of 20 × 30 $cm^2$. To obtain a uniform film for both PTAA and the perovskite layer, we decided to cut the edges, resulting in a final module substrate area of 20 × 20 $cm^2$.

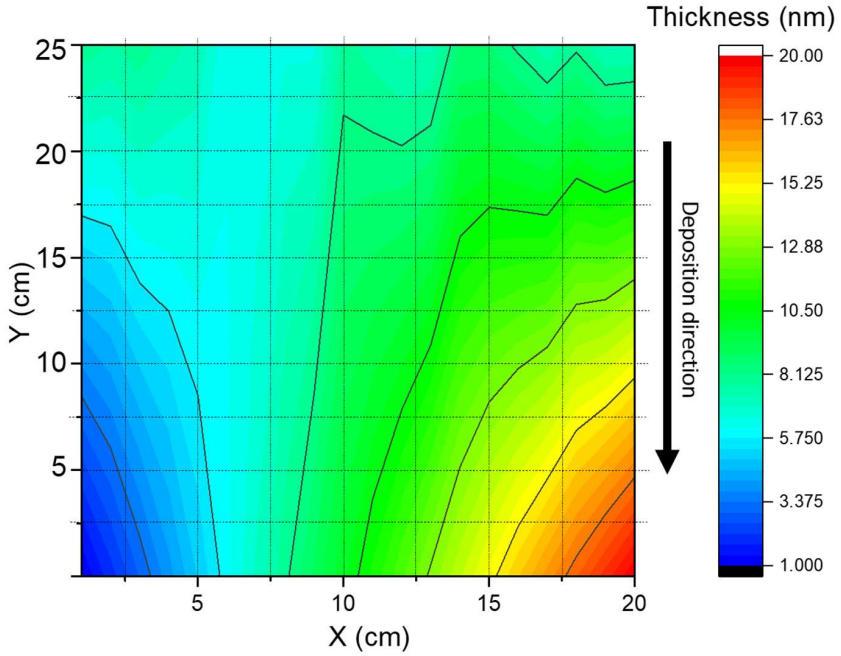


**Figure 2.** Ellipsometry statistic of PET/ITO/PTAA; 5 mg/mL concentration used. Average thickness calculated using standard deviation: 7.6 ± 0.4 nm. Tauc–Lorentz and Gaussian models were used.

**Table 1.** Summary of most of the transparent electrode properties available for third-generation solar cell architectures.

| Transparent Conducting Thin Film | Work Function (eV) | Roughness (nm) | Deposition Method | Electrical Stability |
|---|---|---|---|---|
| $In_2O_3$, $In_2O_3$:Sn (ITO) | 4.1–5.5 | 2–10 | Sputtering | Weak/medium |
| $SnO_2$, $SnO_2$:F (FTO) | 4.2–4.4 | 12–17<br>20–40 | Sputtering<br>Spray | Weak/medium |
| ZnO, ZnO:Al (AZO) | 4.3–4.4 | 40–90 | Oxidation | Weak |
| ZnO, ZnO:In (IZO) | 4.3–4.4 | 8–17 | Sputtering | Weak |
| PEDOT:PSS | 5.1 | 1–5 | Spin-coating | Medium |
| ITO/Ag/ITO | 4.85 | 1–3 | Sputtering | High |
| ZnO/Au/ZnO | 4.80 | 2–4 | Sputtering | High |

#### 3.3.2. Electron Transport Layer

The ETL is required to facilitate efficient electron collection and transportation from the perovskite layer to its respective electrodes. Even though several groups have claimed to obtain PCE of more than 21% for ETL-free devices [24], the incorporation of ETL in perovskite devices is still dominant in terms of efficiency and stability of the devices. For PIN structures, fullerenes are the main materials used to date, and their combination with bathocuproine (BCP) as a buffer layer has been shown to be efficient and stable [25]. Based on our previous work, we decided to conduct panel fabrication using a co-evaporated C60/BCP layer. The reason for this decision is justified by the compactness and the uniform deposition we achieved using co-thermal evaporation, and the fact that this technique reduces the percentage of impurities inside the layer [26]. Evaporation processes can also be used for large substrates, as shown by Li et al. [27], who obtained one of the highest percentages reported for perovskite solar modules, 18.4% on 6.4 $cm^2$.

### *3.4. Counter Electrode*

For the top layer, there are several materials to decide upon for this type of architecture. The best metal may be Ag (silver), due to its work function between 4.2 to 4.7 eV, making it suitable for PIN architectures. However, we decided to use gold (Au), mainly due to the facilitating procedures we developed for the P3 step: we optimized P3 etching of Au on top of inverted structures in our previous work [9], and we also opted for this metal because of its higher conductivity [28]. Ag removal on top of fullerene/BCP and especially C60/BCP when co-evaporated is very difficult to perform when designing the etching for the P3 process, because its removal range is extremely narrowed compared to the Au. For future activities, we could use Ag instead of Au, but precise and meticulous work should be conducted to address the P3 process by laser etching. If the ratio between aperture area and active area of the module could be even lower than 90%, a P3 process could also be conducted by precisely placing a mask before metal evaporation. A summary of all the material choices used for panel fabrication is highlighted in Table 2.

**Table 2.** Summary of the materials used for modules incorporated into the final perovskite panel.

| Layer | Material Choice | Deposition Technique | Main Reason |
|---|---|---|---|
| Substrate and Transparent electrode | Glass/FTO | Pilkington supplier | Robust |
| Perovskite | MA-free | Blade Coating | Intrinsic stable |
| HTL | PTAA | Blade Coating | Thermal stable |
| ETL | C60/BCP | Thermal Evaporation | Compact |
| Counter electrode | Au | Thermal Evaporation | P3 process optimized |

For module fabrication, P1, P2, and P3 processes are required: when increasing the area of a conductive substrate, the resistance is linearly increased, and, to avoid a high series resistance that obstructs the current transport, a series connection of cells is required [11]. We decided to work with a Nd:YVO4 nanosecond laser with $\lambda$ = 355 nm for all three etching steps because of its wider operating windows compared to other wavelengths.

### *3.5. Additional Material for the Panel*

After having chosen all the materials and techniques necessary to fabricate 12 modules with 20 $\times$ 20 $cm^2$ size, we need to consider which additional materials are needed for high-quality panel fabrication. This section might be useful for those who are not familiar with module assembling. Here we list the materials have been used and for what purpose, based on the expertise of our collaboration with Greatcell Energy, who helped us from this stage on. In Table 3, a complete list of the additional materials is highlighted.

**Table 3.** List of additional materials needed for panel fabrication.

| Material | Purpose |
| --- | --- |
| 1 extra clear 3 mm glass sheet 65 × 85 $cm^2$ | Panel Front Screen |
| 1 opaque flexible sheet 65 × 85 $cm^2$ | Panel Backsheet |
| 3 ethylene vinyl acetate (EVA) sheets 65 × 85 $cm^2$ | Panel front and back encapsulants |
| ~12 m of butyl rubber | Lateral sealing |
| 12 non-conductive sheets 18 × 18 cm | Modules protective film |
| 1 Kapton Polyimide Tape | Fix Electric Poles path besides modules |
| | Fix Electric Poles path besides modules |
| 13 Metal conductive 5 cm wires | Module connection |
| 2 Metal conductive 50 cm wires | Electric Poles path |
| 1 Metal conductive tape | Fix metal wires between modules |
| 1 Black Spray Paint | Front Active Area Mask |
| 1 Paper Tape Roll | Cover Panel Active Area from Spray |
| 1 Junction Box | Connect electric pole wires into the final 2 terminal cables |

### *3.6. Lamination Process*

A solar panel lamination process provides protection from adverse environmental conditions, and thus enables a more extended use of solar modules. Lamination provides a hermetically sealed solar panel structure that is durable. The laminate is chemically inert, highly transmissive in the visible spectrum, dimensionally stable at high temperatures, highly resistant to abrasions, and exhibits very little ultraviolet degradation. Our lamination process starts with the front glass: we used extra clear glass of 3 mm in size to reduce any form of UV absorption impacting the charge carrier generation of the modules. Extra clear glass is a type of float glass, which has very low iron content, and is therefore also called low-iron glass.

The iron content in float glass is usually 830–850 ppm (parts per million), while the iron content in an extra clear glass is less than 150 ppm. It allows almost 92% of visible light to be transmitted. Extra clear glass is a colorless transparent glass, and provides a very clear view. The thickness is also a trade-off between robustness and transparency. On top of the extra clear glass, we placed one ethylene vinyl acetate sheet: EVA encapsulation materials have attracted a lot of attention due to their extensive applications in solar cells.

Nearly 80% of silicon and thin film photovoltaic (PV) modules were encapsulated with EVA materials. EVA has many advantages, such as good light transmittance and elasticity, low processing temperature, excellent melt fluidity, and adhesive properties. In addition, their price is relatively low, which makes them very suitable as a solar cell encapsulation materials [29]. We decided to take the 12 modules and connected them following the procedure described in the next section.

### *3.7. Module Connection*

This part of the fabrication process is one of the most delicate to consider: we have to place all modules perfectly aligned and following the correct side and connection path; a picture of the assembling and a scheme is shown in Figure 3.

To prevent any form of damage or delamination of the counter electrode facing up on the assembling step, a non-conductive sheet was placed and fixed using Kapton polyimide film on top of the active area of each module. Modules were connected alternating the correspondent pole using a C-shaped metal-conductive 5 cm wire across two adjacent modules and fixed with metal conductive tape. The conduction was checked via a multimeter, as shown in Figure 3. Any mistake at this stage, by misplacing the side of just one of the modules, results in major failure in the entire process.

To create a conduction path, we need to elongate the positive and negative sides using a couple of 50 cm metal conductive wires, placing them as shown in the scheme in Figure 3. These two wires were eventually placed at the center of the panel, fixing their path in the non-active areas of the modules with Kapton polyimide tape. Later, we placed butyl rubber

all around the edges of the panel inside the size of the extra clear front glass. The thickness of the rubber should be of a couple of millimeters above the thickness of the modules: if it is lower, complete encapsulation is not achieved laterally. Once we placed the rubber and fixed the two wires in the center, we placed two sheets of EVA and the opaque flexible backsheet on top, accurately cutting two tiny squares to allow the wires to come out from the backsheet of the panel. An additional EVA in the top part of the panel was applied to create good isolation between the encapsulant layer and the rubber.

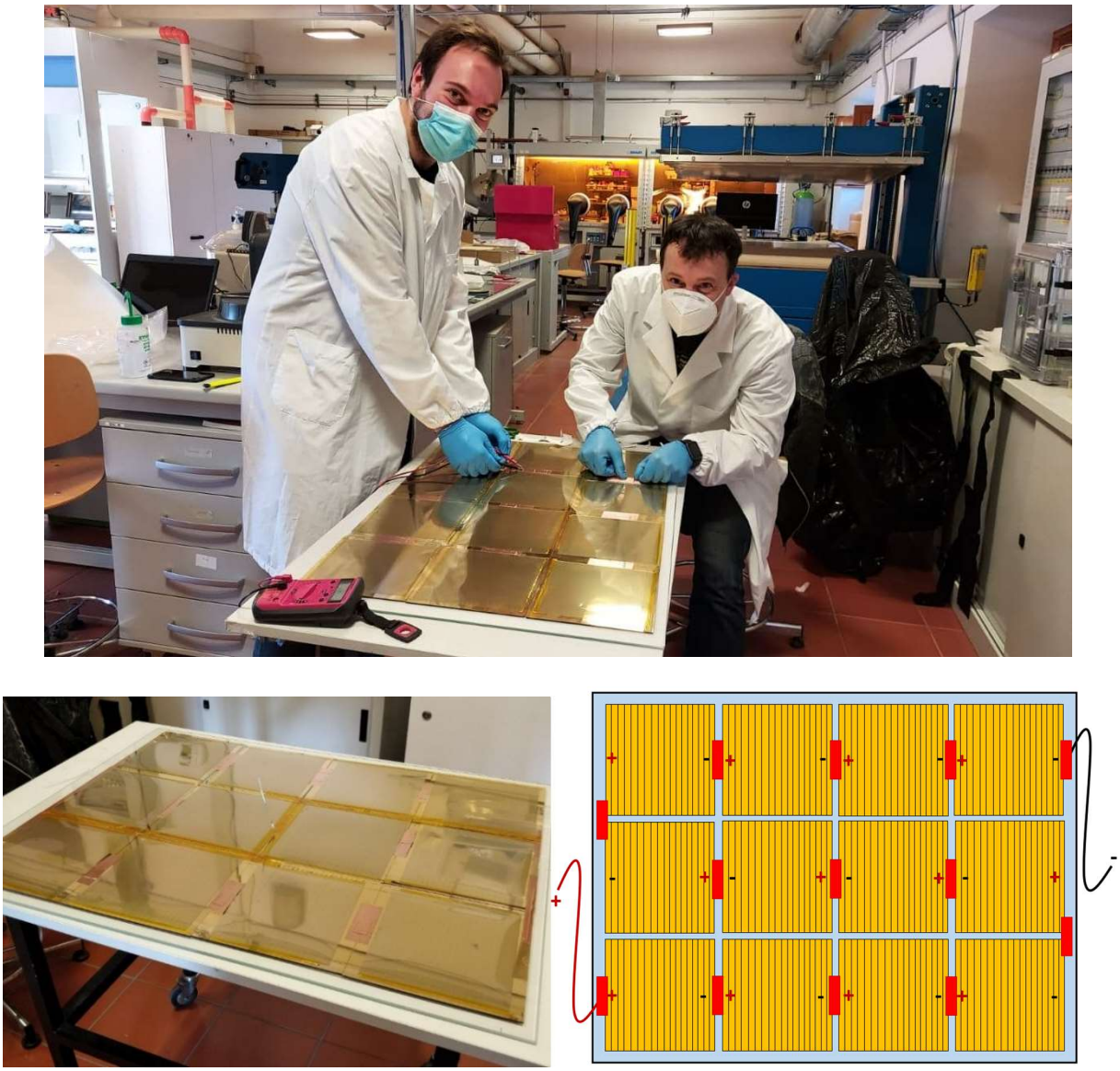

**Figure 3.** (**Top**) Image of Dr. Luigi Angelo Castriotta and Dr. Enrico Leonardi assembling the modules in the panel; (**bottom left**) picture of modules connected prior to the lamination process; (**bottom right**) scheme of the assembled modules. Ph. by Prof. Aldo Di Carlo.

### *3.8. Panel Lamination*

After all materials are in place, the panel is ready to be laminated. In Figure 4 we show the last step before lamination, with the insertion of the opaque flexible backsheet together with the panel placed in the laminator. The lamination process was conducted using an annealing temperature of 85 °C on a heat ramp, with a total lamination time of 60 min. A short video was recorded, which can be viewed in the Supplementary Materials. After 1 h, the panel was well sealed, but two last steps were still required for the fabrication: a mask

needed to be placed to avoid any form of misestimation of the photovoltaic parameters; for this step, we carefully covered the active area of the 12 modules with paper tape, and we then used black spray paint to cover all the inactive areas in black. When the paint is dry, after a minimum waiting time of 1 h, the paper tape was removed: the final panel is shown in Figure 5. As a last step, we connected the junction box at the back of the panel, which is necessary to connect electric pole wires into the final two terminal cables. An additional procedure to use to avoid any breaks at the edges of the front glass is to insert a protection frame all around the panel. In Figure 5, images of the final panel are shown.

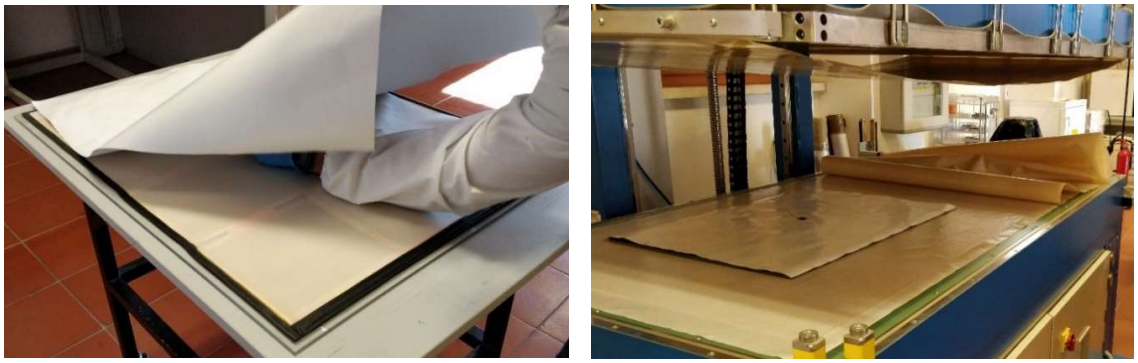

**Figure 4.** On the (**left**), backsheet insertion on the panel; on the (**right**), panel ready to be laminated.


**Figure 5.** Picture of the panel fabricated inside the laboratory (on **top**) and outside (at the **bottom**).

## 4. Discussion

In this work, our aim was to guide the reader through all the steps that need to be considered when fabricating a perovskite solar panel. Nevertheless, before assembling the modules, separate measurement of each module is recommended to check which are the main parameters, and to compile a list of photovoltaic parameters, as shown in the following Table 4 and Figure 6. As shown, Module performances varied from a minimum of 4.05% efficiency and a maximum performing a PCE of 10.4%. The reason of this variation might be related to several factors: the laser processing occurring at a size of over 100 $cm^2$ might create some acceleration mismatch between the beginning and the end of the module, causing different fluence parameters along the length of the scribing. This fluence difference might be especially relevant for P2 and P3 processes, whereas for the P1 process, this is not considered an issue providing the use of higher fluence. The PIN structure and the removal of the HTL/perovskite/ETL layer requires precise control of the P2 laser parameters, although the working range is wider compared to NIP architecture. A difference in fluence parameters along the width of the scribe might be critical for P3 parameters, and especially at the interface between ETL/metal for the PIN structure. This problem creates cell horizontal conduction, revealed by the low Voc measured for some cells along each module. An alternative method to solve this issue might be to use a well-defined mask before metal evaporation deposition, avoiding the use of the laser process for P3. One of the main possible reasons for the low Voc results obtained in the modules might be linked to perovskite deposition: controlling humidity and tempera-ture when processing in air environment is very important, a slight change in these conditions will be reflected in a non-uniform perovskite deposition. The modules that were performing under low currents showed non-uniform perovskite depositions. A possible method to solve this issue might be to deposit perovskite in a more controlled environment.

Unfortunately, our panels did not perform solar-panel-like behavior because of the module degradation that occurred during the lamination step: we speculate that, during lamination, the gold electrode created a bridge and shunted some of the cells inside each of the modules. The mitigation of this effect could be achieved with alternative electrodes that limit possible delamination at the laser process interconnections between cells. An alternative method to solve this issue might be to use a well-defined mask before metal evaporation deposition, avoiding the use of the laser process for P3. One of the main possible reasons for the low $V_{oc}$ results obtained in the modules might be linked to perovskite deposition: controlling humidity and temperature when processing in air environment is very important, a slight change in these conditions will be reflected in a non-uniform perovskite deposition. The modules that were performing under low currents showed non-uniform perovskite depositions. A possible method to solve this issue might be to deposit perovskite in a more controlled environment.

**Table 4.** Photovoltaic parameters of the 12 modules designed with 18 series of connected cells, each with an active area of 201 $cm^2$, assembled in the panel.

| Module Number | FF (%)] | $I_{sc}$ (mA) | $V_{oc}$ (V) | PCE (%) |
|---|---|---|---|---|
| 1 | 42.8 | 101.2 | 19.3 | 7.59 |
| 2 | 44.1 | 86.1 | 18.9 | 6.52 |
| 3 | 38.2 | 94.5 | 18.5 | 5.07 |
| 4 | 35.7 | 99.2 | 18.7 | 5.03 |
| 5 | 62.6 | 98.8 | 18.2 | 10.4 |
| 6 | 42.5 | 72.2 | 18.8 | 4.05 |
| 7 | 45.1 | 71.5 | 18.9 | 4.27 |
| 8 | 44.1 | 71.7 | 18.7 | 4.15 |
| 9 | 46.1 | 71.8 | 18.9 | 4.38 |
| 10 | 47.9 | 86.6 | 18.6 | 8.54 |
| 11 | 50.6 | 80.2 | 17.7 | 8.05 |
| 12 | 46.1 | 107.1 | 16.5 | 9.08 |

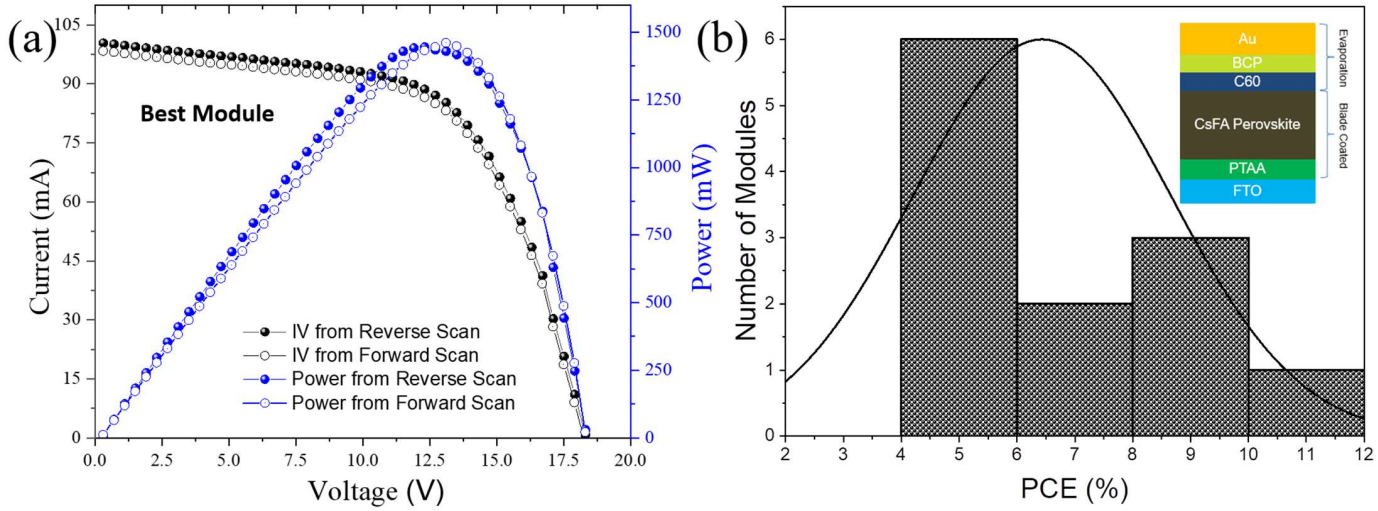


**Figure 6.** (**a**) IV and PV parameters of the best-performing module, with a PCE of 10.4%. (**b**) Statistics of the module performances before the lamination process, with a scheme of the architecture and deposition techniques used.

We further speculate that EVA polymers, even though the lamination temperature used was 85 °C, penetrated up to the perovskite layer and shunted most of the modules, as visible from the diffusion effect on some of the modules (see Figure 5). Even though this effect is not visible on all modules, for a series-connected system, this is sufficient to make a NOT working panel. All 12 modules were displaced in series (see Figure 3): a way to prevent this situation is to use bypass diodes [30], and to design the panel alternating series and parallel connections, to create more chances for a module to work properly by also limiting possible resistive losses that occur due to the amount of bypass diodes inserted into the panel.

## 5. Conclusions

In this work, the feasibility of a perovskite solar panel with a dimension of 0.55 $m^2$ has been described. The choice of materials is fundamental to reduce any possible additional issues that might occur when assembling multiple modules. Modules should be stable enough to ensure the lamination process can be conducted typically from 85 °C onwards, over at least 1 h. The meticulous control of all connections is fundamental to avoid any possible mistakes that are no longer modifiable once the lamination of the panel is complete. Best Module performed 10.4% efficiency on 400 $cm^2$ substrate area, whereas average performances on 12 modules shows an efficiency of 6.3%. When connected and laminated, panel didn't show solar-panel-like behavior because of the module degradation that occurred during the lamination step due to a combination of issues: gold, EVA migration, bypass diodes not used and gradient perovskite deposition in air. Our aim was to demonstrate the feasibility of the process, raising perovskite community on the difficulties and additional issues occurring when assembling a perovskite solar panel.

**Supplementary Materials:** The following supporting information can be downloaded at: https://www.mdpi.com/article/10.3390/pr10101980/s1. Video S1: Lamination process. Figure S1: Picture of the Perovskite film in one of the 20 × 20 $cm^2$ module fabricated; Figure S2: Picture of one Perovskite Module from the glass side; Figure S3: Picture of the Panel back side before the lamination; Figure S4: Pictures of the Panel after lamination (Top and Bottom); Figure S5: Pictures of the Panel in November 2020 (left) and in September 2022 (right).

**Author Contributions:** L.A.C. conceived the work. L.A.C. developed module architecture, design, and fabrication protocol for modules, P1, P2, and P3 processes, as well as film and electrical characterization. E.L. and L.A.C. carried out panel lamination. All authors have read and agreed to the published version of the manuscript.

**Funding:** L.A.C. acknowledge funding from the Italian Ministry of Economic Development in the framework of the Operating Agreement with ENEA for Research on the Electric System.

**Institutional Review Board Statement:** Not applicable.

**Informed Consent Statement:** Not applicable.

**Data Availability Statement:** The data presented in this study are available on request from the corresponding author.

**Acknowledgments:** The authors gratefully acknowledge the financial support of Lazio Region through ISIS@MACH (IR approved by Giunta Regionale n. G10795, 7 August 2019 published on BURL n. 69, 27 August 2019). The authors thank A. Di Carlo for his support and guidance.

**Conflicts of Interest:** The authors declare no conflict of interest.

## References

1. Kim, M.; Jeong, J.; Lu, H.; Lee, T.K.; Eickemeyer, F.T.; Liu, Y.; Choi, I.W.; Choi, S.J.; Jo, Y.; Kim, H.-B.; et al. Conformal quantum dot–$SnO_2$ layers as electron transporters for efficient perovskite solar cells. *Science* **2022**, *375*, 302–306. [CrossRef]
2. Green, M.A.; Dunlop, E.D.; Hohl-Ebinger, J.; Yoshita, M.; Kopidakis, N.; Bothe, K.; Hinken, D.; Rauer, M.; Hao, X. Solar cell efficiency tables (Version 60). *Prog. Photovolt. Res. Appl.* **2022**, *30*, 687–701. [CrossRef]
3. Velilla, E.; Ramirez, D.; Uribe, J.-I.; Montoya, J.F.; Jaramillo, F. Outdoor performance of perovskite solar technology: Silicon comparison and competitive advantages at different irradiances. *Sol. Energy Mater. Sol. Cells* **2019**, *191*, 15–20. [CrossRef]
4. Tress, W.; Domanski, K.; Carlsen, B.; Agarwalla, A.; Alharbi, E.A.; Graetzel, M.; Hagfeldt, A. Performance of perovskite solar cells under simulated temperature-illumination real-world operating conditions. *Nat. Energy* **2019**, *4*, 568–574. [CrossRef]
5. Wu, M.; Haji Ladi, N.; Yi, Z.; Li, H.; Shen, Y.; Wang, M. Stability Issue of Perovskite Solar Cells under Real-World Operating Conditions. *Energy Technol.* **2020**, *8*, 1900744. [CrossRef]
6. Pescetelli, S.; Agresti, A.; Viskadouros, G.; Razza, S.; Rogdakis, K.; Kalogerakis, I.; Spiliarotis, E.; Leonardi, E.; Mariani, P.; Sorbello, L.; et al. Integration of two-dimensional materials-based perovskite solar panels into a stand-alone solar farm. *Nat. Energy* **2022**, *7*, 597–607. [CrossRef]
7. Castriotta, L.A.; Matteocci, F.; Vesce, L.; Cinà, L.; Agresti, A.; Pescetelli, S.; Ronconi, A.; Löffler, M.; Stylianakis, M.M.; Di Giacomo, F.; et al. Air-Processed Infrared-Annealed Printed Methylammonium-Free Perovskite Solar Cells and Modules Incorporating Potassium-Doped Graphene Oxide as an Interlayer. *ACS Appl. Mater. Interfaces* **2021**, *13*, 11741–11754. [CrossRef]
8. Castriotta, L.A.; Fuentes Pineda, R.; Babu, V.; Spinelli, P.; Taheri, B.; Matteocci, F.; Brunetti, F.; Wojciechowski, K.; Di Carlo, A. Light-Stable Methylammonium-Free Inverted Flexible Perovskite Solar Modules on PET Exceeding 10.5% on a 15.7 $cm^2$ Active Area. *ACS Appl. Mater. Interfaces* **2021**, *13*, 29576–29584. [CrossRef] [PubMed]
9. Di Giacomo, F.; Castriotta, L.A.; Kosasih, F.U.; Di Girolamo, D.; Ducati, C.; Di Carlo, A. Upscaling Inverted Perovskite Solar Cells: Optimization of Laser Scribing for Highly Efficient Mini-Modules. *Micromachines* **2020**, *11*, 1127. [CrossRef]
10. Zuo, C.; Bolink, H.J.; Han, H.; Huang, J.; Cahen, D.; Ding, L. Advances in Perovskite Solar Cells. *Adv. Sci.* **2016**, *3*, 1500324. [CrossRef] [PubMed]
11. Castriotta, L.A.; Zendehdel, M.; Yaghoobi Nia, N.; Leonardi, E.; Löffler, M.; Paci, B.; Generosi, A.; Rellinghaus, B.; Di Carlo, A. Reducing Losses in Perovskite Large Area Solar Technology: Laser Design Optimization for Highly Efficient Modules and Minipanels. *Adv. Energy Mater.* **2022**, *12*, 2103420. [CrossRef]
12. Castriotta, L.A.; Infantino, R.; Vesce, L.; Stefanelli, M.; Dessì, A.; Coppola, C.; Calamante, M.; Reginato, G.; Mordini, A.; Sinicropi, A.; et al. Stable Methylammonium-Free p-i-n Perovskite Solar Cells and Mini-Modules with Phenothiazine Dimers as Hole Transporting Materials. *Energy Environ. Mater.* **2022**, e12455. [CrossRef]
13. Wojciechowski, K.; Forgács, D.; Rivera, T. Industrial Opportunities and Challenges for Perovskite Photovoltaic Technology. *Sol. RRL* **2019**, *3*, 1900144. [CrossRef]
14. Mariani, P.; Vesce, L.; Carlo, A.D. A novel class of dye-sensitized solar modules. Glass-plastic structure for mechanically stable devices. In Proceedings of the 2018 IEEE 4th International Forum on Research and Technology for Society and Industry (RTSI), Palermo, Italy, 10–13 September 2018; pp. 1–5.
15. Saliba, M.; Correa-Baena, J.-P.; Wolff, C.M.; Stolterfoht, M.; Phung, N.; Albrecht, S.; Neher, D.; Abate, A. How to Make over 20% Efficient Perovskite Solar Cells in Regular (n–i–p) and Inverted (p–i–n) Architectures. *Chem. Mater.* **2018**, *30*, 4193–4201. [CrossRef]
16. Turren-Cruz, S.-H.; Hagfeldt, A.; Saliba, M. Methylammonium-free, high-performance, and stable perovskite solar cells on a planar architecture. *Science* **2018**, *362*, 449–453. [CrossRef]
17. Gharibzadeh, S.; Fassl, P.; Hossain, I.M.; Rohrbeck, P.; Frericks, M.; Schmidt, M.; Duong, T.; Khan, M.R.; Abzieher, T.; Nejand, B.A.; et al. Two birds with one stone: Dual grain-boundary and interface passivation enables >22% efficient inverted methylammonium-free perovskite solar cells. *Energy Environ. Sci.* **2021**, *14*, 5875–5893. [CrossRef]
18. Khadka, D.B.; Shirai, Y.; Yanagida, M.; Tadano, T.; Miyano, K. Interfacial Embedding for High-Efficiency and Stable Methylammonium-Free Perovskite Solar Cells with Fluoroarene Hydrazine. *Adv. Energy Mater.* **2022**, 2202029. [CrossRef]

19. Bu, T.; Ono, L.K.; Li, J.; Su, J.; Tong, G.; Zhang, W.; Liu, Y.; Zhang, J.; Chang, J.; Kazaoui, S.; et al. Modulating crystal growth of formamidinium–caesium perovskites for over 200 cm2 photovoltaic sub-modules. *Nat. Energy* **2022**, *7*, 528–536. [CrossRef]
20. Reddy, S.H.; Di Giacomo, F.; Di Carlo, A. Low-Temperature-Processed Stable Perovskite Solar Cells and Modules: A Comprehensive Review. *Adv. Energy Mater.* **2022**, *12*, 2103534. [CrossRef]
21. Taheri, B.; De Rossi, F.; Lucarelli, G.; Castriotta, L.A.; Di Carlo, A.; Brown, T.M.; Brunetti, F. Laser-Scribing Optimization for Sprayed SnO2-Based Perovskite Solar Modules on Flexible Plastic Substrates. *ACS Appl. Energy Mater.* **2021**, *4*, 4507–4518. [CrossRef]
22. Serpetzoglou, E.; Konidakis, I.; Kakavelakis, G.; Maksudov, T.; Kymakis, E.; Stratakis, E. Improved Carrier Transport in Perovskite Solar Cells Probed by Femtosecond Transient Absorption Spectroscopy. *ACS Appl. Mater. Interfaces* **2017**, *9*, 43910–43919. [CrossRef] [PubMed]
23. Bi, C.; Wang, Q.; Shao, Y.; Yuan, Y.; Xiao, Z.; Huang, J. Non-wetting surface-driven high-aspect-ratio crystalline grain growth for efficient hybrid perovskite solar cells. *Nat. Commun.* **2015**, *6*, 7747. [CrossRef] [PubMed]
24. Li, D.; Chao, L.; Chen, C.; Ran, X.; Wang, Y.; Niu, T.; Lv, S.; Wu, H.; Xia, Y.; Ran, C.; et al. In Situ Interface Engineering for Highly Efficient Electron-Transport-Layer-Free Perovskite Solar Cells. *Nano Lett.* **2020**, *20*, 5799–5806. [CrossRef]
25. Alsalloum, A.Y.; Turedi, B.; Zheng, X.; Mitra, S.; Zhumekenov, A.A.; Lee, K.J.; Maity, P.; Gereige, I.; AlSaggaf, A.; Roqan, I.S.; et al. Low-Temperature Crystallization Enables 21.9% Efficient Single-Crystal MAPbI3 Inverted Perovskite Solar Cells. *ACS Energy Lett.* **2020**, *5*, 657–662. [CrossRef]
26. Babaei, A.; Dreessen, C.; Sessolo, M.; Bolink, H.J. High voltage vacuum-processed perovskite solar cells with organic semiconducting interlayers. *RSC Adv.* **2020**, *10*, 6640–6646. [CrossRef]
27. Li, J.; Dewi, H.A.; Wang, H.; Lew, J.H.; Mathews, N.; Mhaisalkar, S.; Bruno, A. Design of Perovskite Thermally Co-Evaporated Highly Efficient Mini-Modules with High Geometrical Fill Factors. *Sol. RRL* **2020**, *4*, 2000473. [CrossRef]
28. Gilani, T.H.; Rabchuk, D. Electrical resistivity of gold thin film as a function of film thickness. *Can. J. Phys.* **2018**, *96*, 272–274. [CrossRef]
29. Jiang, S.; Wang, K.; Zhang, H.; Ding, Y.; Yu, Q. Encapsulation of PV Modules Using Ethylene Vinyl Acetate Copolymer as the Encapsulant. *Macromol. React. Eng.* **2015**, *9*, 522–529. [CrossRef]
30. Lan, D.; Green, M.A. Combatting temperature and reverse-bias challenges facing perovskite solar cells. *Joule* **2022**, *6*, 1782–1797. [CrossRef]